Nov 3rd, 12:00 AM

On the Direct Strength Design of Continuous Cold-formed Steel Beams

Cilmar Basaglia

Dinar Camotim

Twentieth International Specialty Conference on Cold-Formed Steel Structures
St. Louis, Missouri, U.S.A., November 3 & 4, 2010

On the Direct Strength Design of Continuous Cold-Formed Steel Beams

Cilmar Basaglia and Dinar Camotim[1]

Abstract

The work reported in this paper concerns an ongoing investigation aimed at developing an efficient methodology to design continuous cold-formed steel beams failing in modes that combine local, distortional and global features. At this stage, it is intended to assess how accurately can the load-carrying capacity of lipped channel continuous (two and three-span) beams subjected to non-uniform bending be predicted by means of the current Direct Strength Method (DSM) design curves. "Exact" ultimate strength values yielded by geometrically and materially non-linear shell finite element analyses are compared with estimates provided by the DSM equations and, on the basis of this comparison, it is possible to identify some features that must be included in a DSM approach applicable to continuous cold-formed steel beams.

Introduction

The vast majority of cold-formed steel members exhibit very slender cross-sections, a feature rendering them highly prone to geometrically non-linear effects, namely those related to local, distortional and global (flexural or flexural-torsional) buckling. Indeed, a fair amount of research work has been recently devoted to the development of efficient design rules for isolated (single-span) members, mostly subjected to uniform internal force and

[1] Department of Civil Engineering and Architecture, IST/ICIST, Technical University of Lisbon, Av. Rovisco Pais, 1049-001 Lisboa, Portugal.

moment diagrams. The most successful end product of this intense research activity is the "Direct Strength Method" (DSM), which (i) has its roots in the work of Hancock (1994), (ii) was originally proposed by Schafer & Peköz in 1998 and (iii) has been continuously improved since (*e.g.*, Schafer 2008). The DSM provides estimates of the load-carrying capacity of cold-formed steel members exhibiting local, distortional or global failure mechanisms, as well as those undergoing local/global interaction – design curves to account for interaction phenomena involving distortional buckling are currently under investigation (*e.g.*, Kwon *et al.* 2009, Silvestre *et al.* 2009). Since the member ultimate strength can be accurately predicted solely on the basis of its elastic (critical) buckling and yield stresses, the DSM is an efficient alternative to the more traditional "effective width method". Following the universal acceptance of the DSM approach to design cold-formed steel members, it has already been included in the latest editions of the corresponding North American (NAS 2007) and Australian/New Zealander (AS/NZS4600 2005) specifications.

Concerning the determination of the member elastic buckling stress, the current application of the DSM relies heavily on the use of finite strip analysis (FSA), easily accessible to a large number of designers, mostly due to the freely available software developed by Schafer & Ádány (2006). However, at the moment FSA can only handle accurately simply supported single-span members subjected to uniform internal forces and moments.

In practice, many cold-formed steel members exhibit multiple spans (*e.g.*, secondary elements such as purlins or side rails) and are often subjected to non-uniform bending moment diagrams combining positive (sagging) and negative (hogging) regions, a feature making their buckling behavior rather complex, as it may (i) combine local, distortional and global features and (ii) involve a fair amount of localization (*e.g.*, the occurrence of local and/or distortional buckling in the vicinity of intermediate supports, where there are relevant moment gradients and little restraint can be offered to the slender bottom/compressed flanges). Even so, it seems fair to say that it is still very scarce the amount of research devoted to the buckling and post-buckling behaviors of cold-formed steel beams subjected to non-uniform bending moment diagrams, namely continuous beams. In this context, it is worth noting the recent works of (i) Yu & Schafer (2007), who used shell finite element models to investigate the influence of linear bending moments on the distortional buckling and post-buckling behaviors of single-span steel beams,

and applied their findings to examine and extend the DSM design procedure to such members, (ii) Camotim *et al.* (2008), who employed Generalized Beam Theory (GBT) to analyze the buckling behavior of steel beams with several loadings and support conditions (including intermediate supports), and (iii) Pham & Hancock (2009), who proposed a DSM-based design criterion for purlin-sheeting systems using elastic lateral-torsional buckling moments evaluated through the so-called C_b-factor approach or finite element analyses.

The objective of this work is to report the available results concerning an ongoing investigation aimed at developing an efficient methodology to design continuous cold-formed steel beams failing in arbitrarily complex collapse modes. The first step consists of assessing how accurately can the ultimate strength of lipped channel continuous (two and three-span) beams subjected to non-uniform bending (due to uniformly transverse loads) be predicted by the current DSM design curves, developed primarily for single-span (isolated) members. In order to achieve this goal, one incorporates into the DSM expressions "exact" (i) critical load factors, evaluated by means of GBT analyses, and (ii) ultimate load (collapse load) factors, obtained from first-order elastic-plastic shell finite element (SFE) analyses carried out in the code ANSYS (SAS 2004). The DSM ultimate strength estimates are compared with "exact" values, yielded by geometrically and materially non-linear SFE analyses, also performed in ANSYS. The paper closes with the discussion of the results obtained – in particular, it is possible to draw some interesting (preliminary) conclusions concerning the features that must be incorporated in a DSM-based design approach applicable to continuous cold-formed steel beams similar to those considered in this work.

DSM Design Procedure

The current DSM approach adopts "Winter-type" design curves, calibrated against experimental and numerical results concerning the ultimate strength of single-span (isolated) members subjected to uniform compression and/or bending. In the case of beams, the nominal bending strengths against local (M_{nl}), distortional (M_{nd}) and global (M_{ne}) failures are given by the expressions

$$M_{nl} = M_y \qquad if \qquad \lambda_l = \sqrt{M_y / M_{crl}} \leq 0.776$$

$$M_{nl} = \left(1 - 0.15\left(\frac{M_{crl}}{M_y}\right)^{0.4}\right)\left(\frac{M_{crl}}{M_y}\right)^{0.4} M_y \qquad if \qquad \lambda_l > 0.776 \quad , \quad (1)$$

$$M_{nd} = M_y \qquad if \qquad \lambda_d = \sqrt{M_y / M_{crd}} \le 0.673$$

$$M_{nd} = \left(1 - 0.22\left(\frac{M_{crd}}{M_y}\right)^{0.5}\right)\left(\frac{M_{crd}}{M_y}\right)^{0.5} M_y \qquad if \qquad \lambda_d > 0.673 \quad , \quad (2)$$

$$M_{ne} = M_y \qquad if \qquad \lambda_e = \sqrt{M_y / M_{cre}} < 0.60$$

$$M_{ne} = \frac{10}{9}\left(1 - \frac{10M_y}{36M_{cre}}\right)M_y \qquad if \qquad 0.60 \le \lambda_e \le 1.336$$

$$M_{ne} = M_{cre} \qquad if \qquad \lambda_e > 1.336 \quad , \quad (3)$$

where (i) λ_l, λ_d, λ_e and M_{crl}, M_{crd} and M_{cre} are *local*, *distortional* and *global* slenderness and elastic critical buckling moment values, and (ii) $M_y = W_y f_y$ is the cross-section first yield moment – W_y is its elastic modulus.

Numerical Investigation: Scope and Modeling Issues

The continuous steel (*E=205GPa* and *v=0.3*) beams analyzed have (i) lipped channel cross-sections (dimensions in fig. 1(a)) and (ii) two or three identical spans (2s and 3s) with lengths *L=2.0m* (B2), *L=4.0m* (B4) and *L=5.0m* (B5). They are subject to a uniformly distributed load applied along the shear centre axis (causing only pre-buckling major-axis bending) and acting on either all spans (all) or just one of them (one) – see figure 1(b). The beam end sections are locally/globally pinned and may warp freely, and all the in-plane cross-section displacements are restrained at the intermediate supports.

Concerning the GBT analysis, the following modelling issues are worth noting:

(i) *Cross-Section Discretization*. Figure 2(a) shows the nodes considered in the lipped channel section. This discretization leads to *17* deformation modes, which are *global* (**1**-**4**), *distortional* (**5**-**6**) and *local* (**7**-**17**) – figure 2(b) shows the in-plane configurations of the most relevant ones.

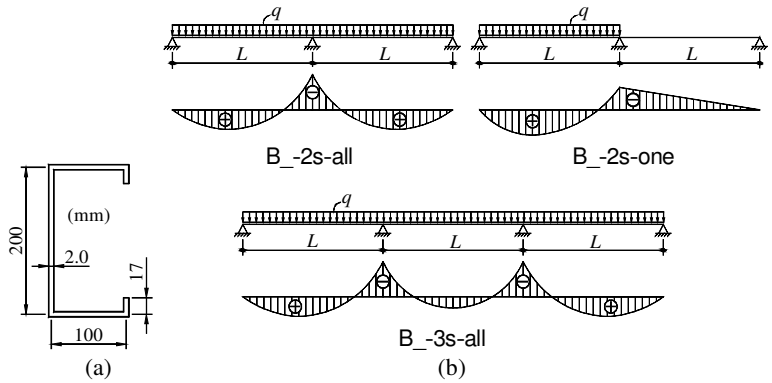

Fig. 1: Continuous beam (a) cross-section dimensions and (b) loading and first-order elastic bending moment diagrams

(ii) *Member Discretisation*. The equilibrium equations were solved using the beam finite element developed by Camotim *et al.* (2008): 2-node elements with 2*n* d.o.f. per node (*n* is the number of deformation modes included in the analysis), and mode amplitude functions approximated by Hermite cubic polynomials. Each beam span was discretized into *20* finite elements in all cases.

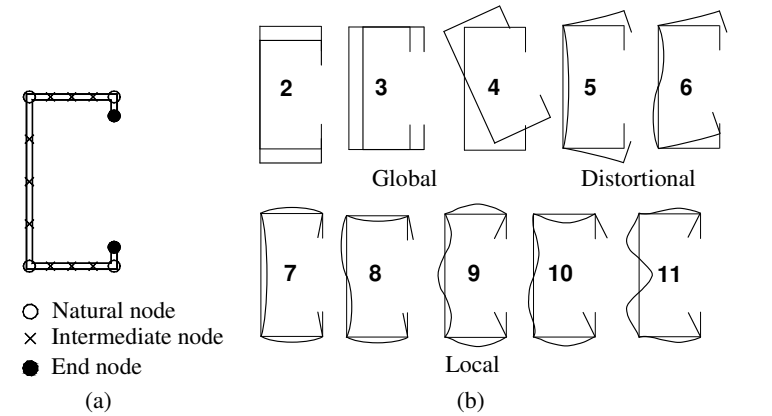

Fig. 2: (a) Lipped channel GBT discretization and (b) in plane shapes of the *10* most relevant deformation modes

Concerning the SFE analyses are concerned, the following issues are relevant:

(i) *Discretization*. The beam mid-surfaces were discretized into SHELL181 finite elements (ANSYS notation: isoparametric 4-node shell elements) – earlier investigations showed the adequacy of these elements. The beam discretization involved *20* elements along the cross-section mid-line and length-to-width ratios of about *1.3* (web and flanges) and *4* (lips).

(ii) *Support Conditions*. The support conditions were modeled in the "usual fashion": null transverse membrane and flexural displacement imposed at all cross-section nodes associated with the end and intermediate supports – in order to preclude the longitudinal rigid-body motion, the axial displacement was prevented at a beam mid cross-section node.

(iii) *Loading*. Transverse load distributions *q'* were applied along the cross-section mid-line covering the whole span length. These transverse loads are (iii_1) statically equivalent to a uniformly distributed load *q* applied along the beam shear centre axis (see fig. 3(a)) and also (iii_2) qualitatively similar to the first moment of the cross-section with respect to the its major axis (see fig. 3(b)).

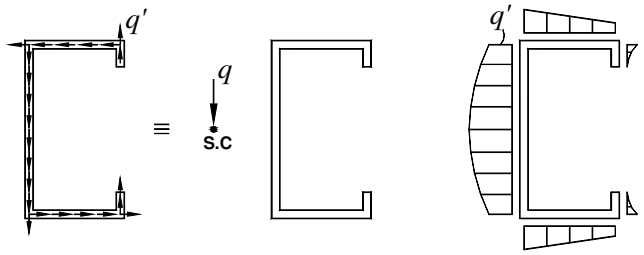

Fig. 3: (a) Applied transverse loads *q'* statically equivalent to a load *q* along the shear centre (S.C) axis and (b) cross-section distribution of the load *q'*

(iv) *Material Modeling*. The steel material behavior was deemed either linear elastic (bucking analyses) or a linear-elastic/perfectly-plastic with a von Mises yield criterion (post-buckling analyses).

(v) *Initial Imperfections*. All initial geometrical imperfections have the beam critical buckling mode shape and amplitude equal to either *10%* of the wall thickness (local/distortional buckling) or *L/1000* (global buckling).

Buckling Analysis

In all existing design procedures, a crucial step is the identification of the buckling mode nature, by no means clear in continuous beams. This can be confirmed by examining figure 4, which provides two representations of the B5-2s-all beam critical buckling mode shapes, namely (i) a 3D-view yielded by an ANSYS SFE analysis and (ii) the GBT modal amplitude functions. Note (i) the excellent agreement between the ANSYS and GBT results and (ii) how the critical buckling mode combines the three deformation mode types: contributions from local (**7**+**8**) and distortional (**5**+**6**) modes, mostly in the close vicinity of the intermediate support, and global (**3**+**4**) modes with higher participations at the mid-span regions.

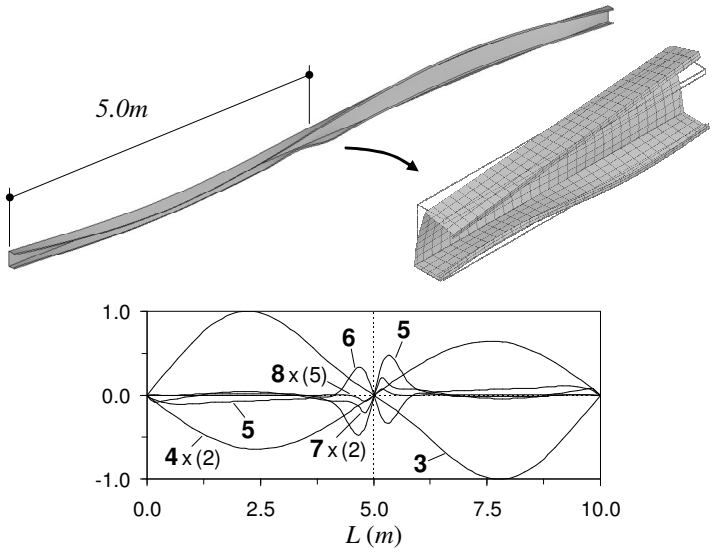

Fig. 4: ANSYS and GBT-based B5-2s-all beam critical buckling mode shapes

In order to attempt to establish the "dominant nature" of the beam critical buckling modes, GBT analyses were carried out including only global (**2**-**4**), distortional (**5**-**6**) and local (**7**-**17**) deformation modes. Table 1 shows the critical load values (q_{cr}), yielded by the ANSYS and GBT (including all deformation modes) analyses, and the relation between the "pure" global ($q_{b.e}$), distortional

($q_{b.d}$) and local ($q_{b.l}$) buckling loads and $q_{cr.GBT}$ – the "dominant buckling mode nature", given in the last column, reflects the "closeness" between the corresponding "pure" buckling load and $q_{cr.GBT}$ (lowest of the three ratios).

Table 1: Relation between the "pure" (q_b) and critical (q_{cr}) load values

Beam	Crit. Load (*kN/m*)		$\frac{q_{b.e}}{q_{cr.GBT}}$	$\frac{q_{b.d}}{q_{cr.GBT}}$	$\frac{q_{b.l}}{q_{cr.GBT}}$	Dominant buckling mode nature
	$q_{cr.GBT}$	$q_{cr.ANSYS}$				
B2-2s-all	46.66	46.78	5.193	1.399	1.032	Local
B4-2s-all	10.82	10.71	1.439	1.104	1.187	Distortional
B5-2s-all	6.06	5.92	1.074	1.172	1.391	Global
B2-2s-one	44.42	44.81	5.091	1.067	1.293	Distortional
B4-2s-one	10.21	10.00	1.416	1.044	1.505	Distortional
B5-2s-one	5.61	5.61	1.073	1.178	1.785	Global
B2-3s-all	53.19	52.42	4.585	1.074	1.021	Local
B4-3s-all	12.35	12.38	1.267	1.046	1.329	Distortional
B5-3s-all	6.13	6.09	1.063	1.303	1.805	Global

Post-Buckling Analysis

The ultimate load values q_u presented in the next sections were obtained through beam elastic-plastic SFE analyses carried out up to failure. To convey the meaning of these values, figure 5 (a) shows the post-buckling equilibrium paths (q *vs.* V_1) of the B2-2s-all beam with different yield stresses (f_y=*250*, *350*,*550*,*850 MPa*) – (i) the symbols □, △, ○ and ◇ indicate the ultimate loads and (ii) V_1 is the displacement selected to provide a better characterization of the beam post-buckling behavior, corresponding to the vertical displacement of the bottom flange-lip corner of the cross-section located in the beam left span, *23.4 cm* away from the intermediate support (see fig. 5(b)). As expected, the amount of post-critical strength reserve increases with the yield stress.

Figure 6 concerns the B2-2s-all beam with f_y=*250 MPa* and displays the deformed configurations and von Mises stress distributions associated with (i) the full yielding of the mid-cross-section (first plastic hinge formation), at q=*33.4 kN/m* (point **I** – fig. 5(a)), and (ii) the beam collapse, at q_u=*37.8 kN/m* (point **II**) and corresponding to the nearly simultaneous yielding of the two mid-span cross-sections. Note the very clear bending moment redistribution.

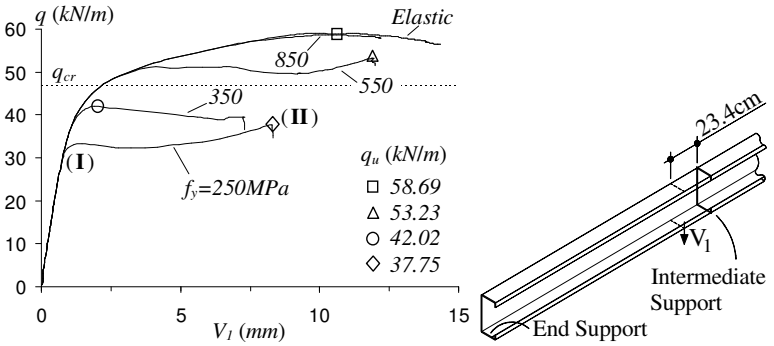

Fig. 5: B2-2s-all beam (a) equilibrium paths and (b) measured displacement

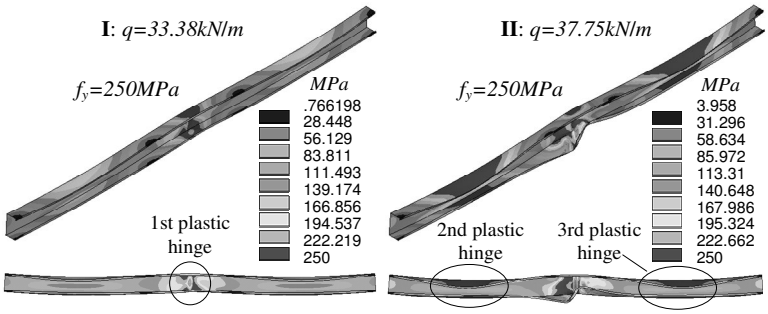

Fig. 6: B2-2s-all beam deformed configuration and von Mises stresses concerning the formation of the first plastic hinge and the beam collapse

Assessment of the DSM Strength Estimates

In beams subjected to non-uniform bending, it is convenient to replace the various "M_y and M_{cr} values" appearing in (1)-(3) by "first yield q_y and critical buckling q_{cr} load values" – in this case, the obvious choices are

$$q_y = M_y / 0.125L^2 \quad q_{cr} = M_{cr} / 0.125L^2 \quad \textit{for beams } \text{B\_-2s-all}$$

$$q_y = M_y / 0.0957L^2 \quad q_{cr} = M_{cr} / 0.0957L^2 \quad \textit{for beams } \text{B\_-2s-one}$$

$$q_y = M_y / 0.1L^2 \qquad q_{cr} = M_{cr} / 0.1L^2 \qquad \textit{for beams } \text{B\_-3s-all} \quad . \quad (4)$$

Note that using expressions (1)-(3) corresponds to neglecting (i) the cross-section elastic-plastic strength reserve, in both statically determinate and indeterminate beams, and (ii) the bending moment redistribution, in statically indeterminate beams – *i.e.*, overly conservative predictions are to be expected in statically indeterminate beams, particularly in the lower slenderness range.

Figures 7 to 9 show comparisons between the ultimate load predictions yielded by the current DSM design curves and the ultimate loads obtained through SFE analyses involving B_-2s-all, B_-2s-one and B_-3s-all beams with *15* different yield stresses, associated with yield-to-critical load ratios q_y/q_{cr} varying from *0.06* to *3.74* and covering a wide slenderness range – these results are summarized in table A1, presented in the Appendix of this paper). The numerical ("exact") ultimate loads, normalized w.r.t. q_y, are identified by the symbols ○, □ and △, for local, distortional and global buckling/failure modes. Since the beams exhibit buckling/failure modes that are not "pure", the DSM curve choice was based on their "dominant buckling mode nature", given in table 1 – however, λ_l, λ_d and λ_e are calculated with the "real" beam critical buckling load q_{cr}, which is neither "purely" local, distortional or global. The observation of these results/comparisons prompts the following remarks:

(i) The DSM predictions are (i_1) excessively safe in the low slenderness range, (i_2) slightly safe in the intermediate slenderness range and (i_3) too unsafe (local and distortional) or moderately safe (global) in the high slenderness range.

(ii) None of the DSM curves provides a set of efficient (safe and economic) predictions of the continuous beam ultimate loads, which is due to a combination of factors: (ii_1) neglecting both the cross-section elastic-plastic strength reserve and (mostly) the moment redistribution (low slenderness range) and (ii_2) the "mixed" nature of the failure mechanisms (high slenderness range).

(iii) Since the beam ultimate loads already incorporate the local, distortional and global buckling effects, it seems to make little sense to neglect the cross-section elastic-plastic strength reserve and moment redistribution. The recent work by Shifferaw & Schafer (2007) partially confirms this assertion, as it reports experimental and numerical evidence, involving simply supported isolated beams (no moment redistribution), of the

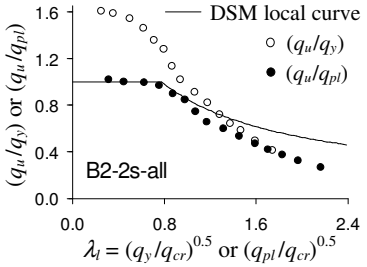

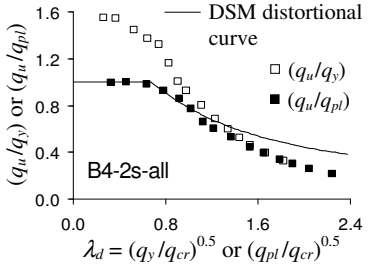

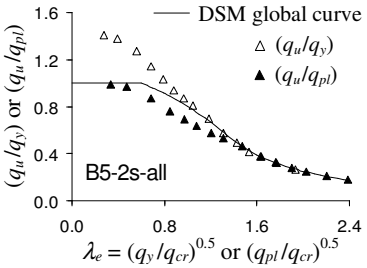

Fig. 7: B_-2s-all beams – comparison between the SFE ultimate loads and DSM design curve predictions

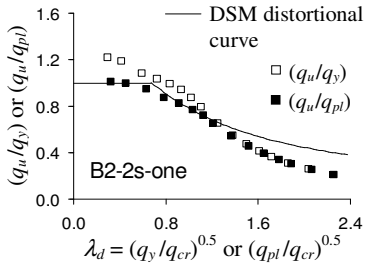

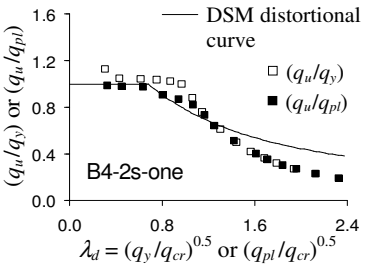

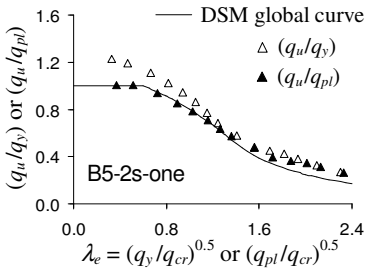

Fig. 8: B_-2s-one beams – comparison between the SFE ultimate loads and DSM design curve predictions

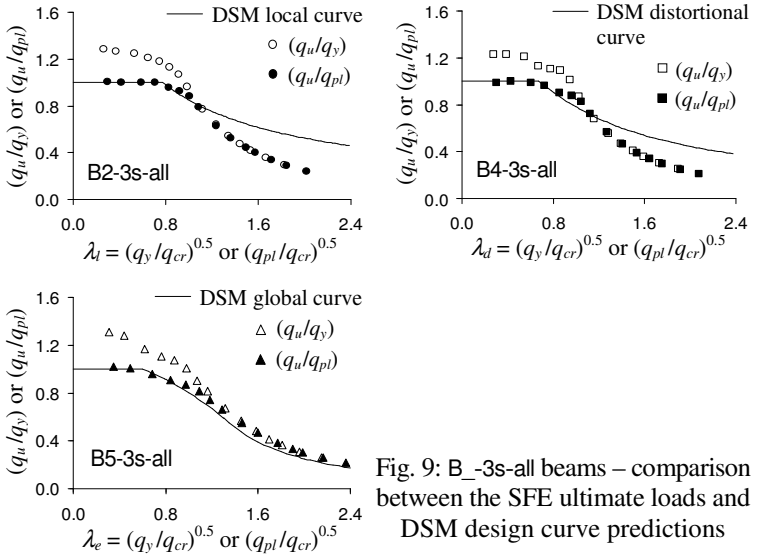

Fig. 9: B_-3s-all beams – comparison between the SFE ultimate loads and DSM design curve predictions

(logical) presence of a non-negligible inelastic strength in the low slenderness range – obviously due to the cross-section plastic strength.

(iv) The most rational approach to account for the beam inelastic strength reserve (including moment redistribution) is to replace the beam *first yield* loads q_y by (geometrically linear) *plastic collapse* loads q_{pl} in (1)-(3). Figures 7 to 9 also compare, for each beam, the ultimate load predictions yielded by the modified DSM design curves with the SFE values, now normalised w.r.t. q_{pl} and represented by the symbols ●, ■ and ▲. Moreover, figures 10 to 11 display all these results grouped according to the beam dominant buckling mode nature. The observation of this new set of results leads to the following comments:

(iv.1) In the low slenderness range, the modified DSM predictions are quite accurate (a few of them are slightly unsafe), which confirms the presence and relevance of the beam inelastic strength reserve.

(iv.2) In the intermediate slenderness range, most of the modified DSM predictions are fairly accurate, although there are a number of slightly unsafe (beams B2-2s-all and B2-2s-one) and safe (beams B4-2s-all, B4-2s-one, B5-2s-one, B2-3s-all, B4-3s-all and B5-3s-all)

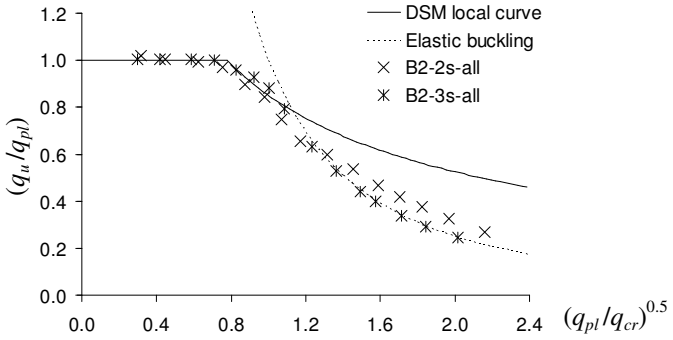

Fig. 10: SFE ultimate loads and modified DSM predictions (local failure)

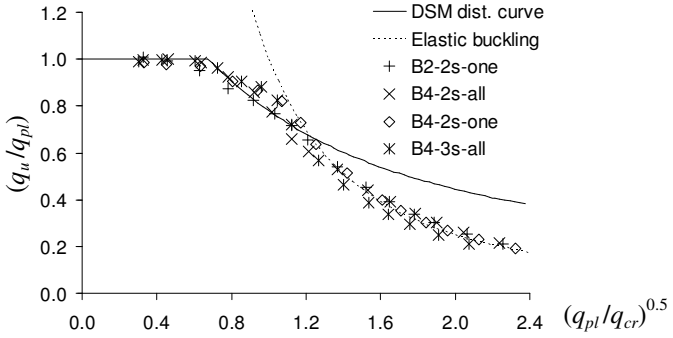

Fig. 11: SFE ultimate loads and modified DSM predictions (distort. failure)

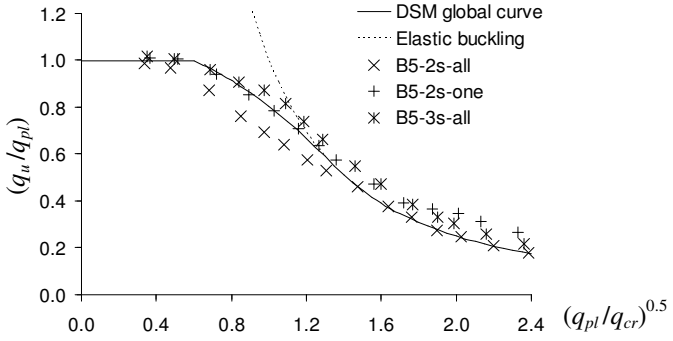

Fig. 12: SFE ultimate loads and modified DSM predictions (global failure)

estimates. The beam B5-2s-all predictions (predominantly global failures) are the exceptions, as they are clearly unsafe.

(iv.3) In the high slenderness range, there is practically no difference between the current and modified DSM predictions, due to the fact that failure stems mainly from stability effects (plasticity plays a lesser role). Indeed, in this slenderness range, the elastic critical buckling curves (dashed lines) provide almost always safe and accurate ultimate load estimates. The exception are now the beam B4-3s-all ultimate loads (predominantly distortional failures), which lie slightly below the corresponding elastic critical buckling curve.

Although considerable more research work is obviously needed before firm guidelines concerning the DSM design of continuous cold-formed steel beams can be established, it is possible to make some preliminary comments on the basis of the limited amount of results presented in this work:

(i) Since there are no "pure" buckling and failure modes, the DSM curve choice should be based on the concept of "dominant buckling/failure mode nature". Nevertheless, the local, distortional and global slenderness values are based on the "real" critical buckling load.

(ii) The first yield load (moment) should be replaced by the first-order plastic collapse load (moment), thus accounting for the cross-section elastic-plastic strength reserve and bending moment redistribution. Failing to do this will inevitably lead to overly conservative prediction in the low-to-intermediate slenderness range.

(iii) Apparently, the most rational approach is to develop and calibrate design curves based on (iii_1) the elastic-plastic collapse load, for stocky beams, and (iii_2) the elastic buckling load, for slender beams. Nothing can yet be said about intermediate beams (or about the slenderness limits separating the three ranges) – nevertheless, the current DSM design curves provide satisfactory ultimate load estimates in this range.

Conclusion

This work reported the available results of an ongoing investigation aimed at developing an efficient methodology to design continuous cold-formed steel beams failing in arbitrarily complex collapse modes. At this stage, it was assessed how accurately can the ultimate strength of continuous lipped channel beams (two and three spans) subjected to non-uniform bending

be predicted by the current DSM design curves. It was found that, in order to achieve a better accuracy, "exact" (i) critical load factors, evaluated by means of GBT analyses, and (ii) ultimate load factors, obtained from elastic-plastic first-order SFE ANSYS analyses, had to be incorporated into the DSM expressions. Then, the (modified) DSM ultimate strength estimates were compared with "exact" values, yielded by geometrically and materially non-linear SFE ANSYS analyses. The following aspects deserve to be mentioned:

(i) The beam buckling and failure modes combine at least two deformation mode types, which precludes a straightforward classification. Thus, one must resort to the "dominant buckling/failure mode nature" concept in order to choose of the appropriate DSM design curve.

(ii) The direct application of the current DSM design curves leads to either overly conservative (stocky beams) or clearly unsafe (slender beams) ultimate load predictions. After a few modifications, the "quality" of the DSM ultimate strength estimates improved significantly.

(iii) The numerical (SFE) ultimate loads obtained clearly indicated that (iii_1) the beams with low-to-intermediate slenderness exhibit a fair amount of inelastic strength reserve, stemming mostly from moment redistribution, and (iv_2) the ultimate loads of the slender beams are fairly well approximated by their critical buckling loads. Although further studies are required to confirm these preliminary findings, it seems that the incorporation of a few modifications in the current DSM design curves will make it possible to account efficiently for these two aspects.

Acknowledgements

The first author gratefully acknowledges the financial support provided by *"Fundação para a Ciência e Tecnologia"* (FCT – Portugal), through the post-doctoral scholarship nº SFRH/BPD/62904/2009.

References

AS/NZS4600 (2005). *Cold-formed Steel Structures.* Australian Standard/New Zealand Standard 4600, Standards Australia, Sydney.

Camotim D, Silvestre N, Basaglia C and Bebiano R (2008). GBT-based buckling analysis of thin-walled members with non-standard support conditions, *Thin-Walled Structures*, **46**(7-9), 800-815.

Hancock GJ, Kwon YB and Bernard ES (1994). Strength design curves for

thin-walled sections undergoing distortional buckling, *Journal of Constructional Steel Research*, **31**(2-3), 169-186.

Kwon YB, Kim BS and Hancock GJ (2009), "Compression tests of high strength cold-formed steel channels with buckling interaction", *Journal of Constructional Steel Research*, **65**(2), 278-289.

NAS (2007). *North American Specification for the Design of Cold-Formed Steel Structural Members* (AISI-S100-07), American Iron and Steel Institute (AISI), Washington (DC).

Pham C.H. and Hancock G. (2009). Direct strength design of cold-formed purlins, *Journal of Structural Engineering*, **135**(3), 229-238.

Schafer BW (2008). Review: the direct strength method of cold-formed steel member design, *Journal of Constructional Steel Research*, **64**(7-8), 766-778.

Schafer BW and Pekoz T (1998). Direct strength prediction of cold-formed steel members using numerical elastic buckling solutions, *Thin-Walled Structures - Research and Development* (ICTWS'98 – Singapore, 2-4/12) N. Shanmugam, J.Y.R. Liew, V. Thevendran (eds.), Elsevier, 137-144.

Schafer BW and Ádány S (2006). Buckling analysis of cold-formed steel members using CUFSM: conventional and constrained finite strip methods, *Proceedings of 18th International Specialty Conference on Cold-Formed Steel Structures* (Orlando, 26-27/10), R. LaBoube, W.W. Yu (eds.), 39-54.

Shifferaw Y and Schafer BW (2007). Inelastic bending capacity in cold-formed steel members, *Proceedings of SSRC Annual Stability Conference* (New Orleans, 18-21/4), 279-299.

Silvestre N., Camotim D. and Dinis P.B. (2009), "Direct strength prediction of lipped channel columns experiencing local-plate/distortional interaction", *Advanced Steel Construction – An International Journal*, **5**(1), 45-67.

Swanson Analysis Systems (SAS) (2004). *ANSYS Reference Manual* (vs. 8.1).

Yu C. and Schafer B.W. (2007). Simulation of cold-formed steel beams in local and distortional buckling with applications to the direct strength method, *Journal of Constructional Steel Research*, **63**(5), 581-590.

Appendix

Table A1 shows the ultimate load predictions yielded by current ($q_{u,y}$) and modified ($q_{u,pl}$) DSM design curves, as well as the "exact" ultimate loads obtained through SFE ANSYS analyses (q_u) of the beams dealt with in this work. Moreover, the beam dominant buckling mode nature (BM), which may be either local (L), distortional (D) or Global (G), is also provided.

Table A1: Comparison between the "exact" beam ultimate load values and the two DSM estimates

Beam	BM	SFE			DSM		$\frac{q_{u.y}}{q_u}$	$\frac{q_{u.pl}}{q_u}$
		q_y	q_{pl}	q_u (kN/m)	$q_{u.y}$	$q_{u.pl}$		
B2-2s-all	L	0.030	0.046	0.047	0.030	0.046	0.62	0.98
		0.059	0.093	0.094	0.059	0.093	0.63	1.00
		0.118	0.183	0.182	0.118	0.183	0.65	1.01
		0.177	0.266	0.258	0.177	0.266	0.69	1.03
		0.236	0.356	0.320	0.236	0.330	0.74	1.03
		0.295	0.447	0.377	0.291	0.385	0.77	1.02
		0.354	0.537	0.401	0.329	0.436	0.82	1.09
		0.413	0.642	0.420	0.366	0.490	0.87	1.17
		0.531	0.812	0.485	0.433	0.572	0.89	1.18
		0.649	0.992	0.532	0.494	0.652	0.93	1.23
		0.768	1.184	0.555	0.552	0.731	0.99	1.32
		0.886	1.359	0.570	0.606	0.799	1.06	1.40
		1.004	1.559	0.587	0.657	0.873	1.12	1.49
		1.181	1.809	0.590	0.730	0.960	1.24	1.63
		1.417	2.184	0.590	0.821	1.083	1.39	1.84
B4-2s-all	D	0.007	0.011	0.011	0.007	0.011	0.65	1.01
		0.015	0.023	0.023	0.015	0.023	0.65	1.00
		0.030	0.043	0.043	0.030	0.043	0.69	1.02
		0.044	0.066	0.061	0.044	0.061	0.73	1.00
		0.059	0.091	0.078	0.056	0.075	0.72	0.97
		0.074	0.111	0.086	0.066	0.086	0.76	1.00
		0.089	0.136	0.089	0.074	0.097	0.83	1.09
		0.103	0.158	0.096	0.082	0.107	0.85	1.12
		0.133	0.201	0.107	0.096	0.124	0.90	1.16
		0.162	0.251	0.111	0.109	0.141	0.98	1.27
		0.192	0.292	0.115	0.120	0.154	1.05	1.34
		0.221	0.342	0.116	0.131	0.169	1.13	1.45
		0.251	0.386	0.117	0.141	0.181	1.21	1.54
		0.295	0.447	0.116	0.155	0.196	1.33	1.69
		0.354	0.537	0.116	0.172	0.217	1.48	1.87
B5-2s-all	G	0.005	0.007	0.007	0.005	0.007	0.71	1.01
		0.009	0.013	0.013	0.009	0.013	0.73	1.03
		0.019	0.028	0.024	0.019	0.027	0.79	1.11
		0.028	0.043	0.032	0.027	0.038	0.84	1.18
		0.038	0.056	0.039	0.035	0.046	0.89	1.19
		0.047	0.069	0.044	0.041	0.052	0.94	1.19
		0.057	0.086	0.049	0.047	0.058	0.94	1.17
		0.066	0.101	0.053	0.051	0.060	0.96	1.13
		0.085	0.128	0.059	0.058	0.061	0.97	1.02

Table A1: Comparison between the "exact" beam ultimate load values and the two DSM estimates (cont.)

Beam	BM	SFE			DSM		$\frac{q_{u.y}}{q_u}$	$\frac{q_{u.pl}}{q_u}$
		q_y	q_{pl}	q_u (kN/m)	$q_{u.y}$	$q_{u.pl}$		
B5-2s-all	G	0.104	0.158	0.060	0.060	0.061	1.01	1.01
		0.123	0.183	0.061	0.061	0.061	1.00	1.00
		0.142	0.213	0.059	0.061	0.061	1.03	1.03
		0.161	0.243	0.061	0.061	0.061	1.00	1.00
		0.189	0.287	0.061	0.061	0.061	1.00	1.00
		0.227	0.337	0.061	0.061	0.061	1.00	1.00
B2-2s-one	D	0.039	0.047	0.047	0.039	0.047	0.82	0.99
		0.077	0.092	0.092	0.077	0.092	0.84	1.01
		0.154	0.176	0.167	0.154	0.176	0.92	1.05
		0.231	0.273	0.239	0.223	0.251	0.93	1.05
		0.308	0.372	0.306	0.272	0.309	0.89	1.01
		0.386	0.472	0.362	0.316	0.360	0.87	0.99
		0.463	0.562	0.403	0.356	0.402	0.88	1.00
		0.540	0.652	0.427	0.392	0.440	0.92	1.03
		0.694	0.832	0.451	0.458	0.510	1.01	1.13
		0.848	1.027	0.465	0.516	0.578	1.11	1.24
		1.003	1.207	0.473	0.570	0.634	1.20	1.34
		1.157	1.409	0.476	0.619	0.693	1.30	1.46
		1.311	1.580	0.478	0.665	0.740	1.39	1.55
		1.542	1.894	0.478	0.730	0.819	1.53	1.72
		1.851	2.259	0.478	0.809	0.904	1.69	1.89
B4-2s-one	D	0.010	0.011	0.011	0.010	0.011	0.89	1.02
		0.019	0.021	0.020	0.019	0.021	0.96	1.02
		0.039	0.041	0.040	0.039	0.041	0.96	1.03
		0.058	0.066	0.060	0.054	0.060	0.91	1.00
		0.077	0.091	0.079	0.066	0.074	0.84	0.94
		0.096	0.117	0.096	0.077	0.087	0.80	0.91
		0.116	0.140	0.102	0.086	0.097	0.85	0.95
		0.135	0.160	0.102	0.095	0.106	0.93	1.03
		0.174	0.206	0.105	0.111	0.123	1.05	1.16
		0.212	0.265	0.105	0.125	0.142	1.18	1.35
		0.251	0.298	0.105	0.137	0.152	1.30	1.44
		0.289	0.348	0.105	0.149	0.166	1.42	1.57
		0.328	0.392	0.105	0.160	0.178	1.52	1.68
		0.386	0.462	0.105	0.176	0.195	1.67	1.85
		0.463	0.552	0.105	0.195	0.215	1.85	2.04

Table A1: Comparison between the "exact" beam ultimate load values and the two DSM estimates (cont.)

Beam	BM	SFE			DSM		$\frac{q_{u.y}}{q_u}$	$\frac{q_{u.pl}}{q_u}$
		q_y	q_{pl}	q_u (kN/m)	$q_{u.y}$	$q_{u.pl}$		
B5-2s-one	G	0.006	0.008	0.008	0.006	0.008	0.82	0.99
		0.012	0.015	0.015	0.012	0.015	0.84	1.00
		0.025	0.029	0.027	0.024	0.028	0.88	1.01
		0.037	0.045	0.038	0.034	0.039	0.89	1.02
		0.049	0.059	0.047	0.041	0.046	0.89	1.00
		0.062	0.075	0.053	0.048	0.052	0.89	0.98
		0.074	0.090	0.057	0.052	0.055	0.91	0.97
		0.086	0.104	0.059	0.055	0.056	0.92	0.94
		0.111	0.137	0.065	0.056	0.056	0.87	0.87
		0.136	0.166	0.065	0.056	0.056	0.86	0.86
		0.160	0.197	0.072	0.056	0.056	0.78	0.78
		0.185	0.227	0.079	0.056	0.056	0.71	0.71
		0.210	0.255	0.080	0.056	0.056	0.70	0.70
		0.247	0.304	0.081	0.056	0.056	0.69	0.69
		0.296	0.355	0.081	0.056	0.056	0.69	0.69
B2-3s-all	L	0.037	0.047	0.047	0.037	0.047	0.78	0.99
		0.074	0.093	0.094	0.074	0.093	0.79	1.00
		0.148	0.183	0.184	0.148	0.183	0.80	1.00
		0.221	0.268	0.269	0.221	0.268	0.82	1.00
		0.295	0.363	0.349	0.295	0.349	0.85	1.00
		0.369	0.451	0.418	0.353	0.405	0.84	0.97
		0.443	0.536	0.473	0.400	0.454	0.84	0.96
		0.517	0.627	0.497	0.443	0.505	0.89	1.02
		0.664	0.812	0.514	0.524	0.599	1.02	1.17
		0.812	0.987	0.521	0.599	0.680	1.15	1.31
		0.959	1.185	0.524	0.668	0.767	1.27	1.46
		1.107	1.318	0.526	0.733	0.821	1.39	1.56
		1.255	1.559	0.526	0.795	0.915	1.51	1.74
		1.476	1.809	0.526	0.883	1.007	1.68	1.91
		1.771	2.159	0.526	0.993	1.127	1.89	2.14
B4-3s-all	D	0.009	0.011	0.011	0.009	0.011	0.81	1.01
		0.018	0.023	0.023	0.018	0.023	0.82	1.00
		0.037	0.045	0.045	0.037	0.045	0.82	1.01
		0.055	0.065	0.063	0.055	0.062	0.88	1.00
		0.074	0.090	0.082	0.068	0.078	0.84	0.96
		0.092	0.114	0.101	0.080	0.092	0.79	0.91

Table A1: Comparison between the "exact" beam ultimate load values and the two DSM estimates (cont.)

Beam	BM	SFE			DSM		$\frac{q_{u.y}}{q_u}$	$\frac{q_{u.pl}}{q_u}$
		q_y	q_{pl}	q_u (kN/m)	$q_{u.y}$	$q_{u.pl}$		
B4-3s-all	D	0.111	0.136	0.112	0.090	0.102	0.80	0.91
		0.129	0.156	0.113	0.099	0.112	0.88	0.99
		0.166	0.198	0.113	0.116	0.129	1.03	1.15
		0.203	0.243	0.113	0.131	0.146	1.17	1.30
		0.240	0.291	0.113	0.145	0.162	1.29	1.44
		0.277	0.333	0.113	0.158	0.176	1.40	1.56
		0.314	0.382	0.113	0.170	0.190	1.51	1.69
		0.369	0.452	0.113	0.186	0.209	1.66	1.86
		0.443	0.532	0.113	0.207	0.229	1.84	2.04
B5-3s-all	G	0.006	0.008	0.008	0.006	0.008	0.76	0.98
		0.012	0.015	0.015	0.012	0.015	0.78	1.00
		0.024	0.029	0.028	0.023	0.028	0.85	1.01
		0.035	0.043	0.039	0.033	0.039	0.84	0.98
		0.047	0.058	0.051	0.041	0.048	0.81	0.94
		0.059	0.073	0.059	0.048	0.054	0.81	0.91
		0.071	0.086	0.064	0.053	0.058	0.84	0.91
		0.083	0.102	0.067	0.057	0.061	0.85	0.90
		0.106	0.131	0.072	0.061	0.061	0.85	0.85
		0.130	0.156	0.074	0.061	0.061	0.83	0.83
		0.154	0.192	0.074	0.061	0.061	0.83	0.83
		0.177	0.222	0.074	0.061	0.061	0.83	0.83
		0.201	0.242	0.074	0.061	0.061	0.83	0.83
		0.236	0.286	0.074	0.061	0.061	0.83	0.83
		0.283	0.342	0.074	0.061	0.061	0.83	0.83